Clinical, pathological and molecular characteristics of patients with disease recurrence despite pathologic response to neoadjuvant ipilimumab plus nivolumab in stage III melanoma

Versluis, J.M.; Shehwana, H.; Elens, R.; Menzies, A.M.; Reijers, I.L.M.; Dimitriadis, P.; ... ; Blank, C.U.

communications medicine

A Nature Portfolio journal

Article

https://doi.org/10.1038/s43856-025-01118-9

Clinical, pathological and molecular characteristics of patients with disease recurrence despite pathologic response to neoadjuvant ipilimumab plus nivolumab in stage III melanoma

Judith M. Versluis[1], Huma Shehwana[2], Robert Elens[3], Alexander M. Menzies[4,5,6], Irene L. M. Reijers[1], Petros Dimitriadis[2], Nigel G. Maher[4,5,7], Astrid M. M. van der Veldt[8], Ellen Kapiteijn[9], Annegien Broeks[3], Richard A. Scolyer[4,5,7,10], Bart A. van de Wiel[11], Alexander C. J. van Akkooi[4,5,12], Ton N. Schumacher[2,13], Georgina V. Long[4,5,6,10] & Christian U. Blank[1,2,9]

Abstract

Background Pathologic response has been shown to be strongly associated with long-term event-free survival after neoadjuvant ipilimumab plus nivolumab in stage III melanoma. Only a small proportion of patients developed disease recurrence after initial pathologic response, making conclusions with statistically significant data challenging. However, the homogeneity of population of patients with stage III melanoma might augment the ability to identify immune resistance mechanisms.

Methods To test if recurrence could be due to true tumor immune evasion or due to insufficient persistence of the immune pressure, 10/140 patients with pathologic response after neoadjuvant ipilimumab plus nivolumab with disease recurrence were identified within the OpACIN, OpACIN-neo, and PRADO trials.

Results Compared to their counterparts without recurrence, clinical characteristics are different regarding sex, age, BRAF mutation status, depth of pathologic response and frequency of immune-related endocrinopathies. Immune activation-related gene expressions are increased at recurrence after major pathologic response (MPR), but not after pathologic partial response (pPR), and TCR diversity nor clonality are different between baseline and recurrence for both MPR and pPR.

Conclusions No genetic changes explaining tumor immune evasion are found. We propose that disease recurrence may potentially be explained by diminishing of the initial therapy-induced immune response, but not due to genetic changes in the tumor cells mediating immune evasion.

Plain language summary

Pathologic response (response assessed in the pathological specimen) to neoadjuvant therapy (treatment before surgery) in patients with melanoma (a type of skin cancer) with lymph node metastases (stage III) usually predicts good long-term outcomes. However, disease recurrence still occurs in a small number of patients. To understand why, patients with such disease recurrence after initial pathologic response were analyzed. Patient data and tumor characteristics such as DNA, RNA, and immune characteristics were assessed. No genetic changes were found that would indicate the tumor cells had developed ways to escape the immune system. This could indicate that the recurrence of the disease was not due to immune evasion, but rather incomplete removal of all tumor cells and weakening of the induced tumor immune response, allowing tumor cells to regrow.

Neoadjuvant immune checkpoint inhibition (ICI) has demonstrated promising results in several cancer types[1–5], and ICI initiation prior to surgery has shown superiority to adjuvant ICI in a phase II trial in melanoma[6]. In macroscopic stage III melanoma, neoadjuvant ipilimumab (anti-CTLA-4) plus nivolumab (anti-PD-1) induced pathologic response rates of 72–78%[7–9], and these high response rates translated into high 3-year recurrence-free survival (RFS) rates of 80–82%[10–12]. In patients with pathologic response (≤50% residual viable tumor), a 3-year RFS rate of 95% has been observed compared to 37% for patients without pathologic response[11], emphasizing the role of pathologic response as a marker of long-term patient benefit.

A full list of affiliations appears at the end of the paper. e-mail: c.blank@nki.nl

As disease recurrence after pathologic response to neoadjuvant ICI is rare, presently no data exist on potential mechanisms of acquired immune resistance in this subset of patients. Taken into account the strong homogeneity of this patient population one might envision that, despite the small patient numbers, resistance mechanisms may potentially be identified. We hypothesized that disease recurrence could be due to true tumor immune evasion (mediated by genetic changes of the tumor cell and thereby allowing grow out of the tumor cells) or due to insufficient persistence of immune pressure (allowing grow out of the tumor without need of genetic changes). In stage IV melanoma it has been shown that loss of beta-2-microglobulin (*B2M*) and mutations in interferon-receptor-associated Janus kinase (*JAK*) 1 and 2, resulting in a lack of response to interferon-gamma, were both mechanisms of acquired resistance[13–15], and these mutations are an example of tumor immune evasion. Vice versa, it has also been shown that insufficient persistence of immune pressure enables tumor cells to escape immune surveillance, which allows disease recurrence or progression[16,17]. This distinction can be of importance for the treatment choice in case of disease recurrence: in case of tumor immune evasion, reinitiation of ICI would not lead to response, while an insufficient persistence of the immune pressure could be reinvigorated by reinitiation of ICI.

In this study, we aimed to gain insight into the mechanisms of immune evasion after initial pathologic response to neoadjuvant ICI in macroscopic stage III melanoma by pooling data of the neoadjuvant OpACIN[7], OpACIN-neo[8], and PRADO trials[9]. Here, we describe the baseline clinical characteristics of patients with disease recurrence after initial pathologic response compared to patients without disease recurrence after pathologic response. Furthermore, we analyzed in-depth paired baseline and recurrent tumor samples through immunohistology, RNA and DNA sequencing analyses in order to test our two hypotheses.

Methods

Patients

Patients treated within the OpACIN trial[7], OpACIN-neo trial[8], or its PRADO extension cohort[9] with pathologic response to neoadjuvant ipilimumab plus nivolumab were screened for subsequent disease recurrence. In these three trials patients were treated with two cycles neoadjuvant ipilimumab plus nivolumab, the details of the dosing regimens are previously described[7–9]. All patients underwent surgery at week 6, for OpACIN and OpACIN-neo this consisted of therapeutic lymph node dissection (TLND), patients in PRADO underwent an index lymph node (ILN; the largest lymph node metastasis at baseline) excision only in case of major pathologic response (MPR), or ILN excision followed by TLND in case of a pathologic partial response (pPR) or pathologic non-response (pNR).

Pathologic response was defined according to International Neoadjuvant Melanoma Consortium (INMC) guidelines within the trials[18]: pathologic complete response (pCR; no residual viable tumor), near-complete response (near-pCR; >0- ≤ 10% residual viable tumor), partial response (pPR; >10- ≤ 50% residual viable tumor) or non-response (pNR; >50% residual viable tumor). The MPR category (≤10% residual viable tumor) consisted of pCR and near-pCR. For patients treated within OpACIN and OpACIN-neo the pathologic response assessment was based on the TLND specimen, for patients treated in the PRADO on the ILN only.

Twelve patients had pathologic confirmed recurrence of disease by 1 July 2022, of the 142 patients with pathologic response. Clinical data was obtained of all patients with a pathologic response.

Revision of pathologic response assessment

Revision of the initial pathologic assessment of the twelve patients with disease recurrence after initial pathologic response was performed by a blinded second pathologist, according to the INMC guidelines[18], to review if these patients were correctly identified as patients with pathologic response. The tumor samples were revised by a blinded pathologist at either Melanoma Institute Australia (MIA; ten Dutch patients reviewed by NM and RAS) or at the Netherlands Cancer Institute (NKI; two Australian patients reviewed by BAvdW). The two Australian patients were first reassessed at MIA and both patients were re-classified as pNR: one patient due to incipient necrosis taken into account as viable tumor instead of necrosis as in the initial response assessment, the other patient due to taking into consideration the extra-nodal tumor deposits in the adipose tissue. Both were at review at NKI scored as pNR as well. Patient 6 would be classified as pNR when considering the combined score of the ILN and the lymph nodes resected during TLND, according to both the NKI and MIA assessment, except that in the PRADO trial all patients' responses were solely based on the ILN response assessment.

There was little variability between the initial and revised response assessments, all patients remained in the same response category, except for the two Australian patients described above [Supplementary Table 1]. The scores for necrosis and fibrosis/fibroinflammatory stroma did also differ <10% for most patients [Supplementary Tables 2 and 3].

In addition, baseline biopsies of these patients were assessed for the presence of viable tumor, fibrosis, and/or necrosis, to see if levels of necrosis at baseline could have influenced the response assessment after neoadjuvant treatment. Five patients had ≥10% necrosis at baseline, in two patients this level was increased at response assessment (amongst whom the patient with incipient necrosis) [Supplementary Table 3]. In the baseline samples of all patients, viable tumor cells were present, which went down after treatment.

Tumor samples

Of the ten patients with confirmed pathologic response, pathologic material for analysis was available, which had to contain a tumor cell percentage of ≥30% and had to be sufficient for RNA and DNA isolation. Fresh-frozen baseline samples and recurrent samples were available for three patients; of two patients a fresh-frozen baseline sample and a formalin-fixed, paraffin-embedded (FFPE) recurrent sample were available; of four patients FFPE baseline and recurrent samples were available; and of one patient FFPE samples at baseline, surgery, and recurrence were available [Supplementary Table 4]. Matching baseline and recurrent samples were available of seven patients for immunofluorescence staining. Of the remaining patients, at least one slide could not be scored due to low presence of tumor cells.

Immunofluorescence staining

Prior to multiplex staining, 3 µm slides were cut on TOMO slides. Slides were dried overnight and stored in 4 °C. Before a run was started, slides were baked for 30 min at 70 °C in an oven. Multiplex staining was performed on a Ventana Discovery Ultra automated stainer, using the Opal Polaris 7-Color Manual IHC Kit (50 slides kit, Perkin Elmer, cat NEL861001KT). Protocol starts with baking for 28 min at 75 °C, followed by dewaxing with Discovery Wash using the standard setting of 3 cycles of 8 min at 69 °C. Pretreatment was performed with Discovery CC1 buffer for 32 min at 95 °C, after which Discovery Inhibitor was applied for 8 min to block endogenous peroxidase activity. Specific markers were detected consecutively on the same slide with the following antibodies, anti-CD3 (SP7, Cat RM-9107-S, ThermoScientific, 1/400 dilution 1 h at RT), anti-CD8 (Clone C8/144B, Cat M7103, DAKO, 1/100 dilution 1 h at RT), anti-CD68 (Clone KP1, M0814, Dako, 1/300 dilution, 1 h at RT), anti-FoxP3 (clone 236 A/47, Cat ab20034, Abcam, 1/100 dilution, 2 h at RT), anti-CD20 (Clone L26, cat M0755, Dako, 1/500 dilution, 1 h at RT), anti-Sox10 (Clone BC34, Cat ACI3099C, Biocure Medical, 1/20 dilution) and anti-MelanA (Clone A103, Cat M7196, Dako, 1/1600 dilution) were co-incubated 2 h at RT. Each staining cycle was composed of four steps: primary antibody incubation, opal polymer HRP Ms +Rb secondary antibody incubated for 1 h at RT, OPAL dye incubation (OPAL480, OPAL520, OPAL570, OPAL620, OPAL690, OPAL780, 1/40, or 1/50 dilution as appropriate for 1 h at RT), and an antibody denaturation step using CC2 buffer for 20 min at 95 °C. Cycles were repeated for each new antibody to be stained. At the end of the protocol slides were incubated with DAPI (1/25 dilution in Reaction Buffer) for 12 min. After the run was finished, slides were washed with demi water and mounted with Fluoromount-G (SouthernBiotech, cat 0100-01) mounting medium.

After staining, slides were imaged using the Phenocyter HT (Akoya). Scans were made with the MOTiF protocol. Using the InForm software

version 2.5.0, the MOTIF images were unmixed into 8 channels: DAPI, OPAL480, OPAL520, OPAL570, OPAL620, OPAL690, OPAL780, and Auto Fluorescence and exported to a multilayered TIFF file. The multilayered TIFFs were fused with HALO software version 3.1 to create one file for each sample.

Image analysis of multiplex images was performed using HALO software (Indica Labs, v2.3) and a HighPlex FL algorithm (Indica Labs, v4.0.2). A random forest classifier was used to classify tissue into tumor (Sox10/MelanA$^+$) and stroma (Sox10/MelanA$^+$). Thresholds were set for CD3 (Opal 520), FoxP3 (Opal 570), CD68 (Opal 620), CD8 (Opal 690), and CD20 (Opal 780). Cells were segmented using DAPI as nuclear detection.

DNA and RNA sequencing

Of fresh-frozen samples when available, and otherwise FFPE sections (10 µm), RNA and DNA were isolated when samples contained sufficient tumor material, based on the pathologist's scoring (≥30% tumor cells of H&E-stained cryostat frozen section). RNA and DNA were simultaneously isolated with the AllPrep DNA/RNA/miRNA Universal isolation kit (Qiagen, 80224) using the QIAcube, according to the manufacturer's protocol.

Transcriptome and whole-exome sequencing was performed by CeGaT GmbH (Tübingen, Germany). Using the KAPA RNA HyperPrep with RiboErase (HMR) & SMART-Seq stranded total RNA (Takara), according to the manufacturer's instructions, transcriptome libraries were generated. Exome libraries were generated using the Twist Human Core Exome Plus (Twist Bioscience). These libraries were sequenced with 2 × 100 bp reads on a NovaSeq 600 system according to the manufacturer's protocols, with a sequence quality value of >93% for transcriptome and >90% for exome libraries. Data were analyzed in the CeGaT analysis pipeline. Briefly, demultiplexing of the sequencing reads was performed with Illumina bcl2fastq (2.20). Adapters were trimmed with Skewer (version 0.2.2)[19]. The quality of FASTQ files was analyzed with FastQC (version 0.11.5-cegat)[20].

DNA sequencing data processing

For the determination of mutational load, DNA from peripheral blood monocular cells was previously isolated and sequenced, as described in ref. 21. FastQC and MultiQC were initially used for quality control of FASTQ files[20,22]. FASTQ files were aligned to the human reference genome (GRCh38) using Burrows-Wheeler aligner[23], followed by marking of duplicate reads by Picard MarkDuplicates. Quality of BAM files was evaluated using Qualimap tool[24]. Subsequently, using GATK BaseRecalibrator base quality scores were recalibrated and single nucleotide variants were called using GATK MuTect2[25].

RNA sequencing data processing

FASTQ files were aligned to the human genome (GRCH38) using the STAR aligner. Strandedness information was obtained using NGSderive tool[22]. Aligned BAM files were further used to extract raw counts using HTseq tool[26]. One sample of a pPR patient did not pass quality control, therefore, this sample and its paired sample were excluded. Raw counts were normalized using TMM normalization factor.

Batch effect removal. Gene expression data was log-transformed before batch correction using log2(count+1). The dataset consisted of 12 FFPE (9 lymph node, 1 brain, 1 bone, 1 small bowel) and 5 fresh-frozen (all lymph node) samples with no common replicate between both batches. Three samples sequenced with the single-end method could not be taken along due to the need for >3 replicates for batch correction and therefore these two patients (one MPR and one pPR patient) had to be excluded as well.

We used a replicate based EBN+ algorithm to remove batch effect using mBatch package in R[27]. The model training subset was selected using two criteria. The first criteria was that training sets should have a similar distribution of histological subtypes within each dataset. All 5 fresh-frozen samples in the dataset were obtained from lymph nodes and belonged to two categories (3 baseline and 2 recurrent samples), hence only lymph node baseline (4 samples) and recurrent (3 samples) FFPE samples were used for batch correction. Thus, 7 FFPE samples and 5 fresh-frozen samples were trained for batch correction. The second criteria was that the batch with a smaller number of samples (fresh-frozen) was batch adjusted while the batch with more number of samples (FFPE) was kept invariant for batch correction.

A trained model was applied to fresh-frozen samples for batch correction. Batch-adjusted data was further used for downstream analysis. Our batch effect algorithm homogenized fresh-frozen and FFPE samples but did not affect the real biological heterogeneity associated with other covariates, including different sample origin, site of recurrence, or pathologic response [Supplementary Fig. 1].

Statistical analyses

Descriptive analyses of clinical characteristics were performed using IBM SPSS Statistics, version 27. One patient with pathologic response died seven months after surgery due to immune-related encephalitis without sign of disease recurrence. This patient was excluded for comparison of patients with pathologic response with versus without disease recurrence.

The tumor mutational burden (TMB) was calculated by summarizing the total number of non-synonymous, somatic mutations per sample with a minimal variant allele frequency of 0.05 (5%). GATK CalculateContamination[28], BAMix[29], and NGSCheckMate[30] were used to evaluate correct normal-tumor pairing and any underlying contamination in the tumor samples. The PolyPhen-2 prediction tool was used to predict possible impact of an amino acid substitution on structure and function of human protein[31].

Spatial analyses were performed using the packages tidyverse[32], spatstat[33], and zoo[34]. Using the Gcross function[33], the nearest staining-positive neighbor cell of a tumor cell was determined, and the area under the curve (AUC) was calculated based on the Gcross function versus the distance from this reference tumor cell. To be able to compare the AUC as a measurement of cumulative distribution, the AUC was determined for a range of 50 µm.

Previously defined RNA signatures were analyzed in transcriptome data: interferon-gamma (IFNγ)[35], interleukin-2 (IL-2)[36], and Batf3 signature[37], and in addition immune subsets according to Danaher[38] and MCP-counter[39] were determined. Gene set enrichment analyses (GSEA) were performed with all human MSigDB Hallmark pathways[40], using fGSEA package in R[41]. Single-sample GSEA analysis was performed using GSVA package in R[42]. For TCR calling in bulk RNA sequencing data, MiXCR library was used[43].

Comparison of median levels of TMB and gene expression between MPR and pPR patients was performed using the Mann-Whitney U test. For comparison of levels at baseline and disease recurrence, the Wilcoxon signed rank test for related samples was used. Plots were generated in both GraphPad Prism (version 8.4.3) and RStudio 2022.

Ethics approval

Patients with disease recurrence after pathologic response were identified from OpACIN trial, OpACIN-neo trial or its PRADO extension cohort, for which patients had given written informed consent. This study was conducted with approval from the institutional review board of the Netherlands Cancer Institute and in accordance with Good Clinical Practice guidelines.

Reporting summary

Further information on research design is available in the Nature Portfolio Reporting Summary linked to this article.

Results

Clinical characteristics of patients with disease recurrence after pathologic response

Initially, 12/142 patients with pathologic response in the OpACIN, OpACIN-neo, and PRADO trials were identified with disease recurrence.

Table 1 | Baseline characteristics of patient with pathologic response with disease recurrence versus without disease recurrence

	Responding patients without recurrence (*n* = 129)		Responding patients with recurrence (*n* = 10)		*p* value
Sex					**0.020**
Male	86	(66.7)	3	(30.0)	
Female	43	(33.3)	7	(70.0)	
Age at randomization in years					**0.020**
Median (IQR)	60.0	(52.0-69.0)	52.0	(46.5-54.0)	
BRAF V600E/K mutation					**0.003**
Mutated	45	(34.9)	9	(90.0)	
Wildtype	71	(55.0)	1	(10.0)	
Unknown	13	(10.1)	0		
Location of affected lymph node					0.312
Axilla	62	(48.1)	2	(20.0)	
Axilla + neck	2	(1.6)	0		
Epitrochlear	1	(0.8)	0		
Groin	37	(28.7)	6	(60.0)	
Neck	27	(20.9)	2	(20.0)	
Sum of diameter target lesions in mm					0.636
Median (IQR)	24.0	(18.0-37.0)	29.0	(18.3-38.3)	
PDL-1 expression on tumor cells					0.995
<1%	52	(40.3)	4	(40.0)	
1–50%	10	(7.8)	1	(10.0)	
>50%	39	(30.2)	3	(30.0)	
Unknown	28	(21.7)	2	(20.0)	
Neoadjuvant treatment regimen					0.221
2× IPI 3 mg/kg + NIVO 1 mg/kg q3w (+2× adjuvant)	6	(4.7)	1	(10.0)	
2× IPI 3 mg/kg + NIVO 1 mg/kg q3w	23	(17.8)	0		
2× IPI 1 mg/kg + NIVO 3 mg/kg q3w	84	(65.1)	9	(90.0)	
2× IPI 3 mg/kg q3w + 2× NIVO 3 mg/kg q2w	16	(12.4)	0		
Surgery at week 6					0.797
Index lymph node excision only	57	(44.2)	4	(40.0)	
Lymph node dissection	72	(55.8)	6	(60.0)	
Radiologic response on neoadjuvant treatment					0.787
Response	82	(63.6)	5	(50.0)	
Stable disease	44	(34.1)	4	(40.0)	
Progression	2	(1.6)	0		
Non-evaluable	1	(0.8)	1	(10.0)	
Pathologic response on neoadjuvant treatment					**0.030**
Major pathologic response	111	(86.0)	6	(60.0)	
Partial response	18	(14.0)	4	(40.0)	
Immune-related grade ≥ 3 adverse events	42	(32.6)	3	(30.0)	0.868
Immune-related endocrinopathies	51	(39.5)	7	(70.0)	0.060
Thyroid immune-related adverse event	43	(33.3)	8	(80.0)	**0.003**
Prednisone usage	56	(43.4)	3	(30.0)	0.408
Second-line immunosuppressives	11	(8.5)	2	(20.0)	0.230

Data are reported as *n* (%) unless indicated otherwise; percentages may not total 100 due to rounding. IQR interquartile range, IPI ipilimumab, NIVO nivolumab, q2w/q3w once every 2/3 weeks. Major pathologic response is defined as ≤10% residual viable tumor, pathologic partial response is defined as >10- ≤ 50% residual viable tumor.

However, after central dual revision of the pathologic response (see Methods and Supplementary Tables 1–3), two patients who were initially attributed a pPR were reclassified to pNR, and therefore excluded from further analyses [Supplementary Fig. 2].

The ten patients with disease recurrence after initial pathologic response were more frequently women (70% versus 30%, $p = 0.020$), were younger (median age of 52 versus 60 years, $p = 0.020$), had more frequently a BRAF V600E/K mutation (90% versus 35%, $p = 0.003$), and had more frequently a pPR (40% versus 14%, $p = 0.030$). They also had more frequently thyroid immune-related adverse events ($p = 0.003$), while neither the frequency of any grade ≥3 adverse events, immune-related endocrinopathies, nor prednisone usage differed between both patients groups [Table 1].

Five patients (50%) recurred with regional metastases and five patients (50%) with distant metastases as their first site of disease recurrence. Of the five patients with regional lymph node metastases, four had undergone ILN excision only [Fig. 1a]. The median time to development of regional recurrences was 6.7 months (range 4.1–15.5), and 4/5 patients had their disease recurrence within one year after surgery. Two patients with regional recurrence developed subsequently distant metastases (muscle and skin): 17.8 and 23.5 months after initial surgery, and 9.9 and 18.4 months after treatment of the regional metastases.

The five patients who recurred with distant metastases had all undergone TLND. The median time to distant metastases was 18.0 months (range 5.0–65.5) after surgery, and 2/5 patients had their recurrence within the first year. Sites of the single organ distant recurrences were brain ($n = 2$), breast, bone, and small bowel.

At data cutoff (February 1, 2024), 5/10 patients were alive without evidence of disease, one patient was alive with disease, and four patients had died from their disease. Of the five patients alive without evidence of disease, three patients had received adjuvant nivolumab after surgical resection of the recurrence, one patient had received combination ICI therapy, and one patient had received targeted therapy, of which the latter both resulted in a complete response [Fig. 1a]. The one patient alive with disease did not respond to ICI monotherapy and was therefore switched to combination ICI therapy. All patients who had died due to disease had not responded to systemic therapy: three patients with BRAF-mutated disease had received targeted therapy, of whom one had received ICI as well, and one patient reinduction of ipilimumab and nivolumab in standard stage IV dose [Fig. 1a].

Baseline tumor markers of patients with pathologic response

Baseline IFNγ signature gene expression and TMB levels have been shown to be predictive of both pathologic response and recurrence in the

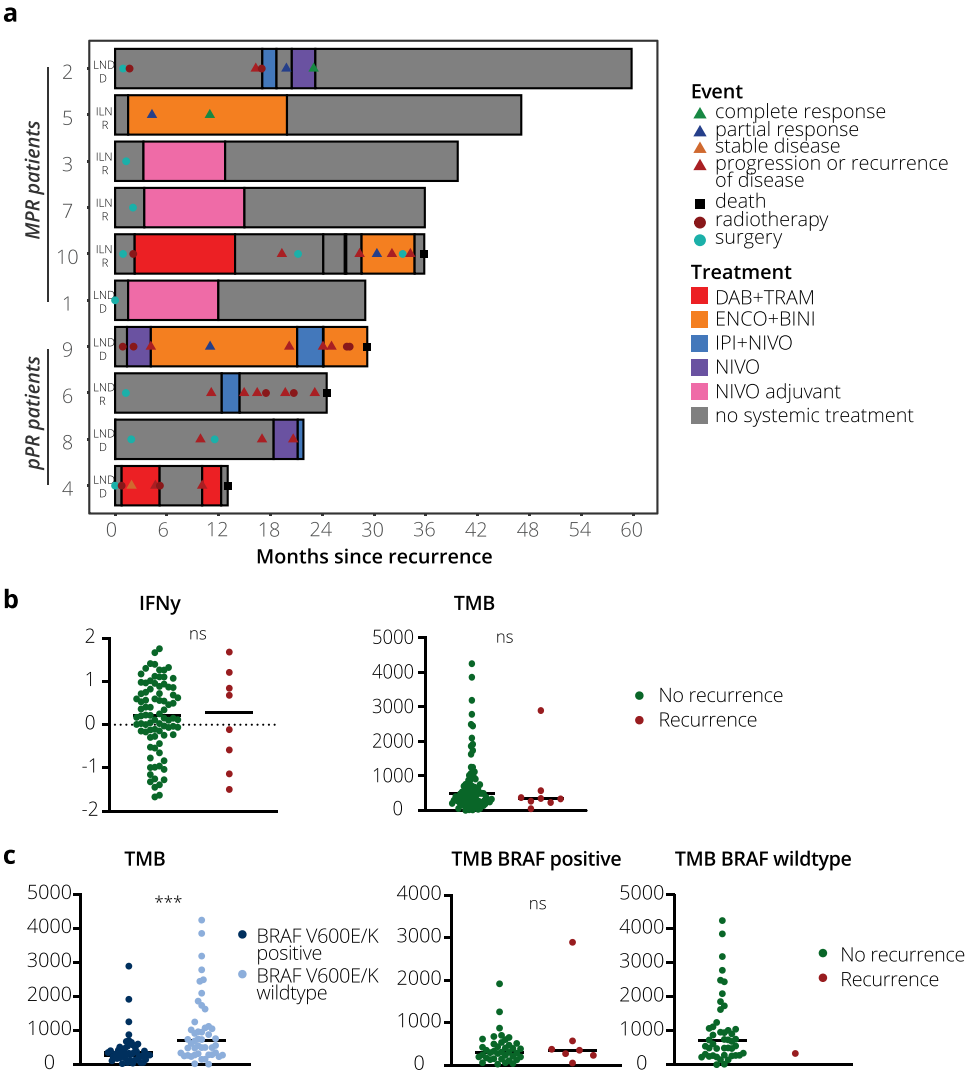

Fig. 1 | Clinical and baseline characteristics. **a** Swimmer plot of subsequent treatment. **b** IFNγ signature gene expression (based on *z*-score) and TMB levels (based on total number of non-synonymous mutations) of patients with pathologic response compared for disease recurrence (with recurrence $n = 8$, without recurrence $n = 85$). **c** TMB levels (based on total number of non-synonymous mutations) for patients with BRAF V600E/K mutation-positive ($n = 46$) and BRAF V600E/K wildtype ($n = 47$) tumors (no recurrence $n = 39$ and $n = 46$, recurrence $n = 7$ and $n = 1$, respectively). D distant recurrence, R regional recurrence, ILN index lymph node resection only, LND therapeutic lymph node resection, DAB + TRAM dabrafenib plus trametinib, ENCO + BINI encorafenib plus trametinib, IPI + NIVO ipilimumab plus nivolumab, NIVO nivolumab, IFNγ interferon-gamma, TMB tumor mutational burden, ns not significant.

neoadjuvant setting in stage III melanoma[21]. Therefore, we have analyzed IFNγ signature and TMB levels for all patients from the three trials in a separate analysis of fresh-frozen baseline tumor samples. Data on both IFNγ signature and TMB levels at baseline were available for 85 patients without recurrence and 8 patients with disease recurrence after pathologic response, and only FFPE material was available from the other two patients. The ratio of recurrence/no recurrence in this subcohort was comparable to the initial patient cohort of the combined trials [Supplementary Table 5].

Neither baseline IFNγ signature nor TMB levels were significantly different between patients with pathologic response and subsequent disease recurrence versus those without, despite a numerical trend towards a lower TMB level in the recurrence group at baseline (median IFNγ 0.2855 versus 0.2034, $p = 0.876$, and median TMB 346.5 versus 484, $p = 0.760$, respectively) [Fig. 1b].

Because BRAF V600E/K mutation was associated with disease recurrence after pathologic response [Table 1], we analyzed baseline TMB levels in the subcohorts of BRAF V600E/K-mutated tumors versus BRAF wildtype tumors from all patients with pathologic response (irrespective of recurrence status). Although there was a significant difference ($p < 0.001$) in TMB levels between patients with BRAF V600E/K-mutated tumors versus wildtype, we found no difference in the subcohorts of BRAF mutation-positive and BRAF wildtype patients when comparing those with versus those without recurrence, with a median TMB level of 245 versus 308.5 in BRAF-mutated tumors and 430 versus 551 for BRAF wildtype tumors, respectively [Fig. 1c].

As the depth of pathologic response was associated with a higher chance of recurrence [Table 1], we analyzed additional pathologic parameters that have previously been associated with outcome on neoadjuvant ICI[44]. We found slightly more viable tumor cells (1.0% versus 0%), more necrosis (7.0% versus 6.0%), less melanophages (0.0% versus 2.0%), and the same level of fibrosis (60.5% versus 61.0%) in the tumor samples of responding patients with recurrence versus those without recurrence [Suppl. Table 6]. All these observations were statistically insignificant, potentially due to the small sample size. Notably, the upper limit of the interquartile range of viable tumor cells was evidently higher in patients with recurrence (19.5% versus 3.0%) and, in contrast, that limit of pigment-laden macrophages was evidently lower in patients with recurrence (3.5% versus 20.0%). This corresponds both with the correlation of the depth of pathologic response with recurrence in our cohort [Table 1] and with the overall analysis including patients without pathologic response[44].

Tumor characteristics at baseline versus disease recurrence

To examine genetic changes as a possible explanation of development of disease recurrence, we analyzed the mutational landscape of the baseline versus recurrent tumor samples. Matched DNA sequencing data were available for all ten patients (six patients with MPR and four with pPR).

In patients who had a pPR, median TMB levels were identical with a total of 316 non-synonymous mutations at baseline versus 311 at recurrence. For the patients with an MPR, median TMB level was lower at baseline compared to the moment of recurrence (157 non-synonymous

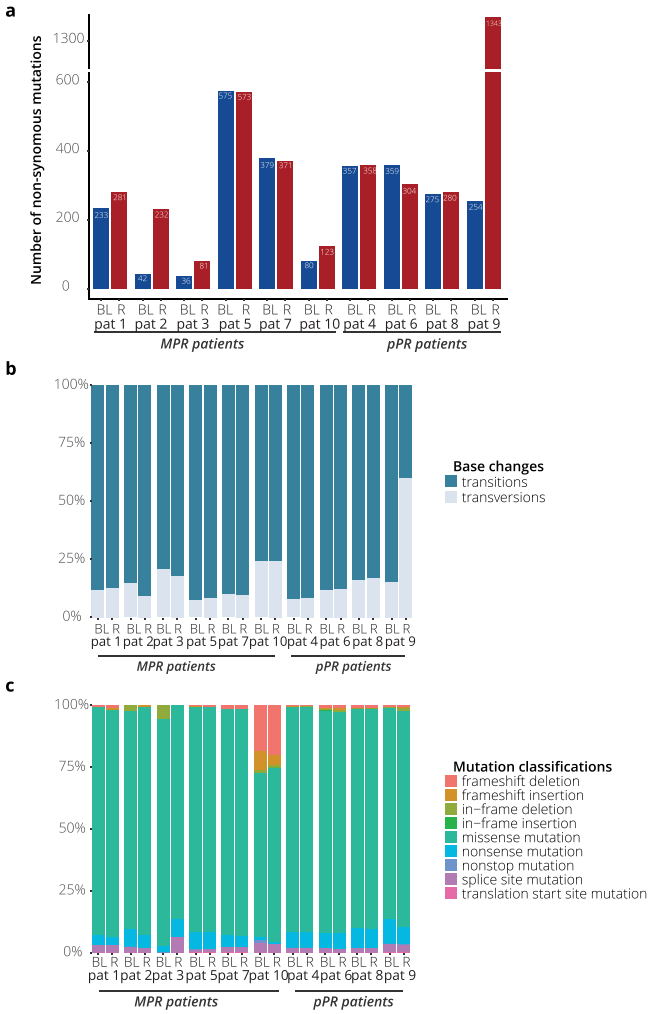

Fig. 2 | Tumor characteristics. a TMB levels of MPR and pPR patients. **b** Base changes, depicted as transitions versus transversions, of MPR and pPR patients. **c** Classification of mutations of MPR and pPR patients. BL baseline tumor sample, R recurrent tumor sample, pat patient, MPR major pathologic response, pPR pathologic partial response.

mutations versus 267), of whom 3/6 MPR patients had evidently higher TMB levels at recurrence [Fig. 2a]. MPR patients had lost a median of 20 mutations (interquartile range [IQR] 10–35) in the recurrent tumor compared to the baseline sample and had gained 69 new mutations (IQR 15–114), while pPR patients had lost a median of 45 (IQR 7–169) and had gained 20 mutations (IQR 9–972) in the recurrent versus baseline sample.

The median number of transversions was slightly lower for MPR patients with 20 (IQR 7–36) at baseline and 27 (IQR 19–36) at recurrence, while for pPR patients no difference was observed (38, IQR 29–42 versus 40, IQR 30–591) [Fig. 2b]. The number of splice-site mutations between baseline (4, IQR 1–7) and recurrence (6, IQR 4–7) was different for MPR patients, as well as the number of missense (134, IQR 36–391 versus 236, IQR 83–386) and non-sense mutations (6, IQR 1–24 versus 11, IQR 5–23). For pPR patients, only in-frame deletions were different between baseline (1, IQR 0–1) and recurrence (3, IQR 1–10) [Fig. 2c].

Patient 9, with an initial pPR, was an outlier patient, with an increase of >1000 in TMB level in the recurrent tumor lesion in the bone. This patient had lost 78% of mutations from the baseline sample and gained 96% new mutations, and displayed the largest difference in mutational profile [Fig. 2B]. All tumor samples included in our analyses had high concordance levels and were matched for each patient.

Based on literature research[13,15,45], we analyzed a list of genes previously related to immune evasion [Supplementary Table 7]. In 5/10 patients no mutations in these genes were found. Four patients had such mutations in both samples, thus these mutations were unlikely to explain the immune evasion resulting to occurrence of disease recurrence [Supplementary Table 8]. New mutations possibly contributing to immune evasion in the recurrent sample, not present in the baseline sample, were found in two patients. MPR patient 10 had gained a frame-shift mutation in the *ATM* gene (involved in DNA damage response), in addition to a frame-shift deletion in *PTEN*. Patient 9 had gained new (and damaging according to PolyPhen prediction[31]) missense variants in *CALR* (has a role in quality control in endoplasmic reticulum via calreticulin/calnexin cycle[46]), *NLRC5* (regulator of MHC-I dependent immune response[47]), and *PIAS4* gene (transcriptional regulator of amongst others, STAT pathway[48]), aside from benign missense variants in *HLA-A*, *HLA-C*, *NLRC5*, and *PTEN* [Supplementary Table 8].

To investigate whether the potential damaging mutations of patient 9 led to altered RNA and subsequent protein expression, we analyzed the RNA sequencing data. RNA gene expression based on z-score for *CALR*, *NLRC5*, and *PIAS4* was increased in the recurrent sample compared to baseline [Supplementary Table 9]. *CALR* (calreticulin) is of importance for the assembly and cell surface expression of MHC class I molecules[49] and *NLRC5* (NOD-like receptor C5) has been shown to induce the expression of *HLA-A*, *HLA-B*, *HLA-C*, *PSMB9*, *TAP1*, and *β2M*[47,50]. RNA gene expression of these genes demonstrated an increase at recurrence as well [Supplementary Table 9]. *PIAS4* (protein inhibitor of activated STAT 4) interacts with p53[48], which is regulated by interleukin-6 (IL-6) and induces STAT3 (signal transducer and activator of transcription 3) binding activity[51]. Expression according to the single-sample GSEA of the Hallmark pathways of p53 (0.075 versus −0.167) and of IL6-JAK-STAT3 signaling (0.150 versus 0.040) was increased at recurrence compared to baseline. In fact, both were in the top 10 of upregulated pathways at recurrence for patient 9, with the IFN-α and IFNγ pathways also included in the top 3 upregulated pathways.

Thus, all these mutations did not result in function-impairing downstream effects in the bulk RNA sequencing data. A remaining challenge is the fact that we cannot differentiate between tumor and stromal cells, as no single-cell RNA sequencing data and no sufficient material for further analyses were available.

Immune characteristics at baseline versus disease recurrence

As no evident explanations for immune evasion were found in our DNA sequencing analyses, we postulated that, instead of a tumor mutation-mediated immune evasion, a decrease in immune infiltration might contribute to disease recurrence. Therefore, we performed multiplex immunofluorescence stainings on matched samples of patients from whom we had sufficient tumor material after DNA and RNA sequencing (four MPR and three pPR patients).

MPR tumors had a higher tumor immune infiltration at baseline compared to recurrence, which was not observed in pPR patients [Fig. 3a]. In detail, the median percentage for MPR patients of $CD3^+$ cells was 9.4% versus 4.3%, $CD8^+$ 6.2% versus 3.5%, $FoxP3^+$ 1.4% versus 0.3%, and $CD20^+$ 0.8% versus 0.2% at baseline versus recurrence, respectively. In contrast, more $CD68^+$ cells were found in the tumors at recurrence: 2.0% at baseline versus 5.0% at recurrence.

In pPR patients, all immune cells had a lower median tumor infiltration at baseline compared to recurrence: $CD3^+$ 0.7% versus 9.9%, $CD8^+$ 1.8% versus 4.1%, $FoxP3^+$ 0.2% versus 1.2%, $CD20^+$ 0.1% versus 0.2%, and $CD68^+$ 0.4% versus 5.0% [Fig. 3a].

However, a pure description of the number of tumor-infiltrated cells cannot differentiate between bystander and tumor-specific immune cells. In an effort to make the distinction, we analyzed the spatial correlation of immune and tumor cells by determining the distance between a tumor cell and the nearest staining-positive neighbor cell, described in the AUC of the Gcross function. An increase of AUC indicates that immune cells lie farther away from reference tumor cells.

For MPR patients, the AUC of $CD68^+$ cells was larger at recurrence, while for $CD3^+$, $FoxP3^+$, and $CD20^+$, the AUC was smaller; thus, these cells

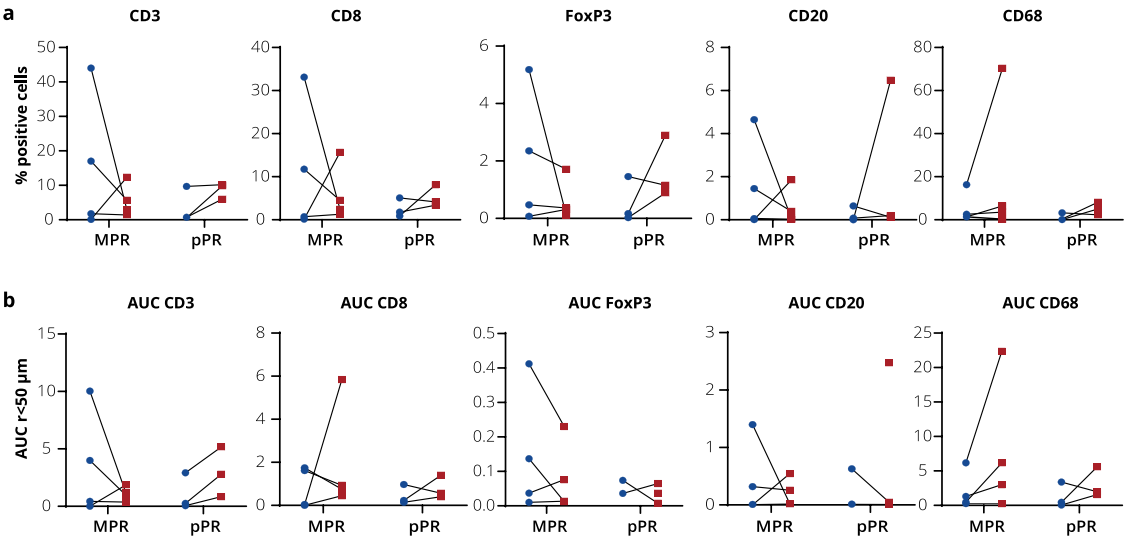

Fig. 3 | Multiplex immunofluorescence. a Percentage of positive cells at baseline (blue) and recurrence (red) as classified by multiplex immunofluorescence, reported for MPR ($n = 4$) and pPR ($n = 3$) patients. **b** Area under the curve at baseline (blue) and recurrence (red), calculated by the Gcross function, as measure of distance between tumor cell and nearest neighbor staining-positive cell, reported for MPR ($n = 4$) and pPR ($n = 3$) patients. MPR major pathologic response, pPR pathologic partial response, AUC area under the curve, µm micrometer.

were in closer proximity to the tumor cells. In contrast, for pPR patients the AUC was generally larger at recurrence, thus all immune cells lay farther away from the tumor cells, except for $CD20^+$ cells [Fig. 3b]. In detail, for MPR patients, the median AUC was at baseline 2.2, 0.1, and 0.2 and at recurrence 1.1, 0.0, and 0.1 for $CD3^+$, $FoxP3^+$, and $CD20^+$ cells, respectively. For $CD8^+$ cells median AUC was stable (0.8), for $CD68^+$ cells median AUC was 0.9 at baseline and 4.6 at recurrence. For pPR patients, median AUC was smaller at baseline than at recurrence for $CD3^+$ cells (0.3 versus 2.8), $CD8^+$ (0.2 versus 0.6), $FoxP3^+$ (0.1 versus 0.0), and $CD68^+$ cells (0.4 versus 2.0). For $CD20^+$ cells, the median AUC was 0.3 at baseline and 0.0 at recurrence [Fig. 3b].

Thus, recurrent tumors seem to have decreasing percentages of immune cell infiltration after MPR and increasing percentages after pPR. Concerning the proximity of immune cells to tumor cells, the inverse phenomenon was observed: despite less $CD3^+$ cells at recurrence compared to baseline after MPR, these immune cells were in closer proximity, indicating a potential larger number of tumor-specific T cells, while the larger number of $CD3^+$ cells, but farther away, at recurrence after pPR, is more indicative of bystander T cell infiltration.

This raised the question of whether the closer proximity observed at disease recurrence actually reflected a stronger immune activation. As no additional material for further analyses was available, for e.g., PD-1, CD45RA/RO, or CD69 immunohistochemistry stainings, we used RNA sequencing data. Matched RNA sequencing data were available for seven patients (four MPR and three pPR patients).

Previously, IFNγ, CD4/IL-2, and Batf3 signatures have been associated with response to neoadjuvant ICI and event-free survival[21,36,52]. Therefore, we analyzed whether changes in the expression levels of these signatures could explain tumor immune evasion despite the initial response. The median z-score of IFNγ signature gene expression demonstrated an increase from 0.249 to 0.447 for MPR patients and only marginal changes for pPR patients (0.452–0.534). The expression of IL-2 and Batf3 gene signatures was increased (median z-score of 0.134–0.213 and 0.225–0.271) at recurrence for MPR patients, whereas the expression was lower at recurrence in pPR patients (median z-score of 0.724–0.456 and 0.422–0.047) [Fig. 4a–c].

These immune signatures seem to confirm the pattern of increase in immune activation at disease recurrence compared to baseline levels after MPR, which is not seen after pPR, although numbers are low. The multiplex data were in line with the gene expression of immune subsets for two MPR patients, confirming the technical reliability [Supplementary Figs. 3 and 4].

This was not the case for the two pPR patients. However, with only two patients in each group for comparison, the sample size was extremely small.

To assess additional possible pathways of immune evasion mechanisms, RNA sequencing data were subsequently analyzed for Hallmark pathway enrichment[40] comparing recurrent with baseline samples for MPR and pPR patients separately. In the four MPR patients, allograft rejection was most enriched at recurrence (normalized enrichment score [NES] of 2.24) [Fig. 4d]. All immune processes except for coagulation were also enriched at recurrence, with allograft rejection, IFNγ response (NES = 1.98), inflammatory response (NES = 1.75), and IL6-JAK-STAT3 signaling (NES = 1.74) as the top 4 upregulated Hallmark pathways. In pPR patients different patterns were observed with epithelial mesenchymal transition (NES = 2.21), angiogenesis (NES = 1.73), and glycolysis (NES = 1.72) as strongest upregulated pathways at recurrence, while allograft rejection was the most downregulated pathway (NES = −1.75) [Fig. 4e].

These data indicate that immune activation is stronger at disease recurrence, which was more prominent after an initial MPR. This may support the notion that despite less immune infiltration after MPR, the closer proximity of immune cells to tumor cells reflects a stronger immune response.

Finally, we investigated TCR clonality to assess a possible difference in the breadth of the T cell response, as we hypothesized that a decline in immune repertoire could explain the disease recurrence. As TCR calling was performed on the raw RNA sequencing data, matched data were available from seven patients (four MPR and three pPR patients).

Complementarity-determining region 3 (CDR3) metrics were not different between baseline and recurrent samples for both MPR and pPR patients. A wide range for TCR diversity was observed, with higher median levels at recurrence for MPR patients (37, IQR 3-243 at baseline versus 97, IQR 25-208 at recurrence), but lower levels at recurrence for pPR patients (91, IQR 11-NR versus 19, IQR 16-NR) [Fig. 5a]. The clonality was not different between time points with a change in median normalized Shannon–Wiener index of 0.939–0.949 for MPR patients and 0.967–0.960 for pPR patients. All patients had at recurrence a normalized Shannon-Wiener index of <1, implying that there were oligoclonal repertoires in the tumor samples, although with all indices >0.8 this was not determined by a small number of dominant clones [Fig. 5b]. Only two MPR patients had shared TCR clones (10–12) between baseline and recurrence [Fig. 5c]. This resulted in a Jaccard index of <0.05 for both patients, so almost no similarity was found between the TCR repertoires at both time points of each patient.

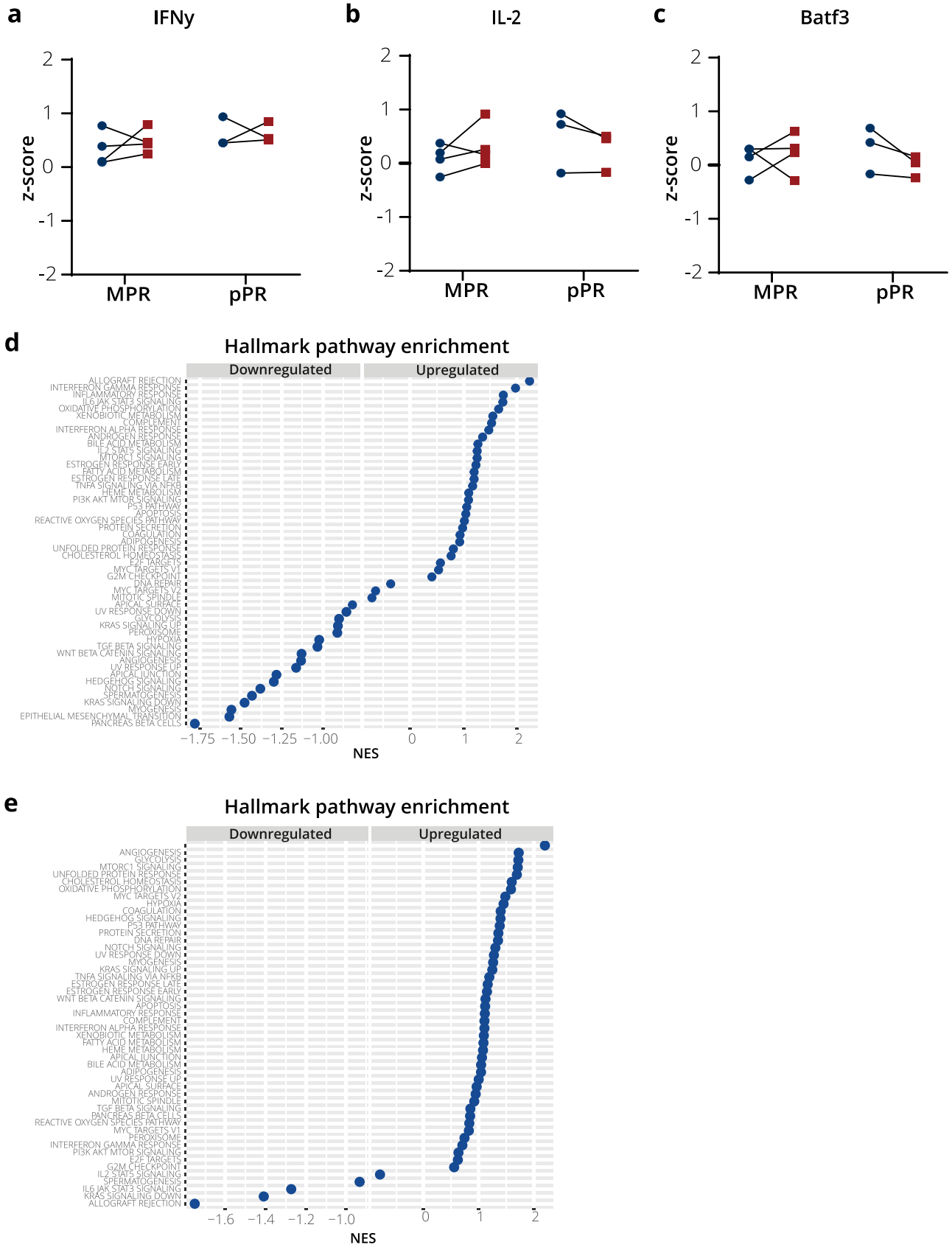

Fig. 4 | Transcriptional data regarding immune characteristics. a IFNγ score of baseline (blue) and recurrence (red) samples, reported for MPR ($n = 4$) and pPR ($n = 3$) patients. **b** IL-2 score of baseline (blue) and recurrence (red) samples, reported for MPR ($n = 4$) and pPR ($n = 3$) patients. **c** Batf3 score of baseline (blue) and recurrence (red) samples, reported for MPR ($n = 4$) and pPR ($n = 3$) patients. **d** Enrichment of Hallmark pathways for MPR patients, reported as either upregulated or downregulated in tumor sample at disease recurrence compared to baseline tumor sample. **e** Enrichment of Hallmark pathways for pPR patients, reported as either upregulated or downregulated in tumor sample at disease recurrence compared to baseline tumor sample. IFNγ interferon-gamma, IL-2 interleukin-2, MPR major pathologic response, pPR pathologic partial response.

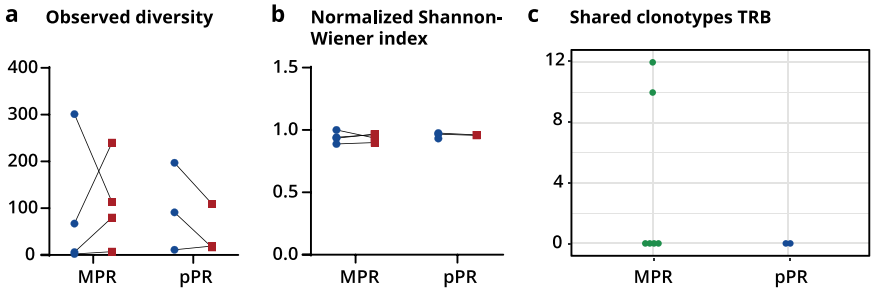

Fig. 5 | T cell receptor characteristics. a Observed diversity of baseline (blue) and recurrence (red) samples, reported for MPR ($n = 4$) and pPR ($n = 3$) patients. **b** Normalized Shannon-Wiener index of baseline (blue) and recurrence (red) samples, reported for MPR ($n = 4$) and pPR ($n = 3$) patients. **c** Shared clonotypes between baseline and recurrence samples, reported for MPR ($n = 4$) and pPR ($n = 3$) patients. MPR major pathologic response, pPR pathologic partial response, TRB T cell receptor beta chain.

In summary, at disease recurrence after initial MPR, more TCR diversity was observed with similar clonality compared to baseline, while after initial pPR there was less diversity and similar TCR clonality compared to baseline, which makes T cell clone depletion less likely to be the mechanism of immune evasion.

At baseline, during response and at disease recurrence

A major challenge for interpretation of our data is the lack of on-treatment samples. One might postulate that the minor differences observed between baseline and disease recurrence represent not an active tumor immune evasion, but a return towards baseline levels and thus an insufficient immune response to restrict tumor growth. If this is true, an on-treatment biopsy should demonstrate an evidently higher immune activation compared to both baseline and recurrence levels. In the only patient of whom we had tumor material between baseline and recurrence (pPR patient 4), this idea is supported. Two additional tumor samples were available for this patient: one of the responding ILN at week 6 (directly after neoadjuvant treatment), and one of a non-responding lymph node resected at week 9.

We found higher immune infiltration at response compared to both baseline and recurrence, with in the responding ILN higher percentages of $CD8^+$, $CD3^+$, and $CD68^+$ cells compared to both baseline and recurrence. In addition, the $CD8^+$ T cells were in closer proximity to tumor cells at response than at recurrence. Both observations are indicative that the immune response at recurrence was diminished towards baseline levels (Supplementary Fig. 5). Furthermore, higher expression of IFNγ and IL-2 signatures was detected in the responding ILN compared to the non-responding lymph node, baseline, and recurrence, while the Batf3 signature remained unchanged (Supplementary Fig. 6). A higher level of TCR diversity was observed in the responding ILN, while a comparable level to baseline is seen at all other time points (Supplementary Fig. 7). At all time points, however, the Shannon-Wiener index was comparable (range 0.958–0.990). In line with our two-time point analyses, the TMB level did not change over time (Supplementary Fig. 8).

Taken together, these data indicate that the neoadjuvant ICI induced an increased immune response sufficient to mediate regression in responding lesions, that diminishes over time and thereby allows recurrence in patients with a pathologic response, probably from not eliminated micrometastases.

Discussion

Understanding the mechanisms of disease recurrence despite initial response to neoadjuvant ICI could be the basis for novel salvage therapies. In this study, we characterized our small but homogeneous cohort of patients who had disease recurrence after initial pathologic response to neoadjuvant combination ICI for stage III melanoma.

These patients with disease recurrence were more often women and younger, were more likely to have a BRAF V600E/K mutation, and more often had a pPR than MPR. Notably, these patients had more frequently thyroid-related adverse events. These factors might not be independent observations, as in advanced melanoma thyroid adverse events were more often observed in women and younger patients, but when adjusted for age, sex, brain metastases, and ICI type, progression-free survival of patients with thyroid adverse events was not different from patients who remained euthyroid[53].

Due to the long-term sustainability of response to neoadjuvant ICI in the vast majority of patients[9,11], tumor material from patients with disease recurrence after initial response is limited available. Therefore, our work lacks statistically significant observations and must be considered as hypothesis-generating only.

We found no genetic changes mediating tumor immune evasion in the tumor samples at recurrence. This is in contrast to data from late-stage melanoma, in which mutations in *B2M*, *JAK1*, and *JAK2*[13–15] or other mutations resulting in HLA loss were suggested to mediate immune evasion. However, these genetic changes have not been confirmed in larger cohorts as commonly observed escape mechanisms yet[54].

As we could not explain the disease recurrence after pathologic response to neoadjuvant ICI by genetic changes in the tumor cells, we have characterized the immune response itself. Again, we did not find striking differences between baseline and recurrence regarding immune infiltration and activation. This is in contrast to the previously described presence of T cells at disease recurrence, although these cells were restricted to the tumor margin[13].

Both the absence of genetic alterations mediating tumor evasion and the comparable immune infiltration characteristics in baseline and recurrent samples led us to the assumption that the occurrence of a clinically detectable recurrence is due to an initially incomplete clearance of all tumor cells despite the initial pathologic response. This could allow disease recurrence due to the diminishing of the ICI-induced immune response. We could confirm this idea in one patient from whom we had additional tumor samples. Indeed, an increase of immune infiltration and activation compared to baseline was observed, which returned to near-baseline levels at the moment of recurrence. Of note, the resected non-responding lymph node demonstrated similar lower immune activation levels as the recurrent sample in this patient.

These data are in line with studies in stage IV melanoma[55] and in the neoadjuvant setting[56], which demonstrated an increase of immune cells, especially $CD8^+$ cells, during treatment compared to baseline. However, in these analyses, data on recurrent tumor samples were missing. Our data are the first effort to fill this knowledge gap.

Notably, more patients with pPR had disease recurrence after pathologic response. This suggests that less efficient tumor killing during the neoadjuvant treatment period, which results in a lesser depth of pathologic response (i.e., pPR instead of MPR), results in an increased risk of disease recurrence. Based on the absence of evidence that these tumor cells develop genetic resistance mechanisms, our data suggest that a longer treatment in pPR patients (e.g., during the neoadjuvant period or additional adjuvant period) might prevent recurrences. Furthermore, our data suggest that reinitiation of ICI in patients with recurrence should be able to re-induce a response to ICI. Indeed, when comparing patient cohorts from different trials (with identical inclusion criteria), additional adjuvant PD-1 blockade seemed to reduce the recurrence rate in patients without pathologic response to neoadjuvant combination ICI[9] compared to patients without pathologic response receiving no adjuvant therapy[21]. Nonetheless, in this current patient cohort with disease recurrence after initial pathologic

response, not all patients responded to ICI reinitiation. Rechallenge with the combination ICI resulted in a response in 1/2 patients, while rechallenge with anti-PD-1 monotherapy resulted in a response in none of the two patients. However, the three patients who had surgery followed by adjuvant anti-PD-1 had no subsequent disease recurrence. Thus, in total, 4/7 patients seem to have benefited from ICI reinitiation.

Our observations that patients with recurrence after pathologic response to neoadjuvant ICI can respond to the same ICI again is contrary to the preclinical concept of immune editing[57]. Moreover, our data suggest that tumors can escape from a diminishing immune response without a change in their immunogenicity.

A missing link in our work is the full characterization of the TCR repertoire by single-cell TCR sequencing and the corresponding neoantigen repertoire. As TMB correlates with the neoantigen repertoire, one might envision that latter analyses are of less relevance. We could not exclude intratumor heterogeneity[58], as our data are based on bulk sequencing data of biopsy material of the baseline and recurrent tumor mass. The different sites of the tumor lesions and the difference in immunogenicity depending on the organ in which the metastasis developed[59–61] could also have interfered, which we could not exclude in our analyses, restricted by the scarcity of material.

Nevertheless, our work is the first attempt to deconvolute immune evasion after pathologic response to neoadjuvant combination ICI. Our data indicate that these rare events do not evolve from genetic changes of the tumor cells, reducing their immunogenicity, nor due to reduced immune infiltration, indicative of chemokine level changes in the tumor microenvironment. Our data propose more likely an insufficient clearance of all tumor cells during the initial neoadjuvant ICI, with an equilibrium between the induced immune response and tumor cells, and subsequently resurfacing of tumor cells after diminishing of the immune response towards baseline levels. A longer neoadjuvant treatment period in patients with pPR, adjuvant therapy in non-MPR patients (as tested in the NADINA trial[62]), or re-challenge with the same ICI or dose-escalated combination ICI at recurrence for patients without MPR or with recurrence after neoadjuvant ICI, could be potential approaches.

Reporting summary

Further information on research design is available in the Nature Portfolio Reporting Summary linked to this article.

Data availability

RNA and DNA sequencing data generated during the study are deposited in the European Genome-phenome Archive (EGA) under the accession code EGAS50000000488. To minimize the risk of patient re-identification, de-identified individual patient-level clinical data are available under restricted access. Upon scientifically sound request, data access can be obtained via the NKI's scientific repository at repository@nki.nl, which will contact the corresponding author (C.U.B.). Data requests will be reviewed by the institutional review board of the NKI and will require the requesting researcher to sign a data access agreement with the NKI.

Received: 31 January 2025; Accepted: 27 August 2025;
Published online: 30 September 2025

References

1. Chalabi, M. et al. Neoadjuvant immunotherapy leads to pathological responses in MMR-proficient and MMR-deficient early-stage colon cancers. *Nat. Med.* **26**, 566–576 (2020).
2. van Dijk, N. et al. Preoperative ipilimumab plus nivolumab in locoregionally advanced urothelial cancer: the NABUCCO trial. *Nat. Med.* **26**, 1839–1844 (2020).
3. Forde, P. M. et al. Neoadjuvant PD-1 blockade in resectable lung cancer. *N. Engl. J. Med.* **378**, 1976–1986 (2018).
4. Schmid, P. et al. Pembrolizumab for early triple-negative breast cancer. *N. Engl. J. Med.* **382**, 810–821 (2020).
5. Vos, J. L. et al. Neoadjuvant immunotherapy with nivolumab and ipilimumab induces major pathological responses in patients with head and neck squamous cell carcinoma. *Nat. Commun.* **12**, 7348 (2021).
6. Patel, S. P. et al. Neoadjuvant-adjuvant or adjuvant-only pembrolizumab in advanced melanoma. *N. Engl. J. Med.* **388**, 813–823 (2023).
7. Blank, C. U. et al. Neoadjuvant versus adjuvant ipilimumab plus nivolumab in macroscopic stage III melanoma. *Nat. Med.* **24**, 1655–1661 (2018).
8. Rozeman, E. A. et al. Identification of the optimal combination dosing schedule of neoadjuvant ipilimumab plus nivolumab in macroscopic stage III melanoma (OpACIN-neo): a multicentre, phase 2, randomised, controlled trial. *Lancet Oncol.* **20**, 948–960 (2019).
9. Reijers, I. L. M. et al. Personalized response-directed surgery and adjuvant therapy after neoadjuvant ipilimumab and nivolumab in high-risk stage III melanoma: the PRADO trial. *Nat. Med.* **28**, 1178–1188 (2022).
10. Blank, C. U. et al. 3-year relapse-free survival (RFS), overall survival (OS) and long-term toxicity of (neo)adjuvant ipilimumab (IPI) + nivolumab (NIVO) in macroscopic stage III melanoma (OpACIN trial). *Ann. Oncol.* **30**, V535 (2019).
11. Versluis, J. M. et al. Survival update of neoadjuvant ipilimumab plus nivolumab in macroscopic stage III melanoma in the OpACIN and OpACIN-neo trials. *Ann. Oncol.* **34**, 420–430 (2023).
12. Reijers, I. L. M. et al. The impact of response-directed surgery and adjuvant therapy on long-term survival after neoadjuvant ipilimumab plus nivolumab in stage III melanoma: three-year data of PRADO and OpACIN-neo. *J. Clin. Oncol.* **41**, 101 (2023).
13. Zaretsky, J. M. et al. Mutations associated with acquired resistance to PD-1 blockade in melanoma. *N. Engl. J. Med.* **375**, 819–829 (2016).
14. Restifo, N. P. et al. Loss of functional beta 2-microglobulin in metastatic melanomas from five patients receiving immunotherapy. *J. Natl. Cancer Inst.* **88**, 100–108 (1996).
15. Sade-Feldman, M. et al. Resistance to checkpoint blockade therapy through inactivation of antigen presentation. *Nat. Commun.* **8**, 1136 (2017).
16. Dunn, G. P. et al. Cancer immunoediting: from immunosurveillance to tumor escape. *Nat. Immunol.* **3**, 991–998 (2002).
17. Swann, J. B. & Smyth, M. J. Immune surveillance of tumors. *J. Clin. Investig.* **117**, 1137–1146 (2007).
18. Tetzlaff, M. T. et al. Pathological assessment of resection specimens after neoadjuvant therapy for metastatic melanoma. *Ann. Oncol.* **29**, 1861–1868 (2018).
19. Jiang, H. et al. Skewer: a fast and accurate adapter trimmer for next-generation sequencing paired-end reads. *BMC Bioinformatics* **15**, 182 (2014).
20. Andrew, S. *FastQC: a quality control tool for high troughput sequence data*. http://www.bioinformatics.babraham.ac.uk/projects/fastqc/ (2010).
21. Rozeman, E. A. et al. Survival and biomarker analyses from the OpACIN-neo and OpACIN neoadjuvant immunotherapy trials in stage III melanoma. *Nat. Med.* **27**, 256–263 (2021).
22. Ewels, P. et al. MultiQC: summarize analysis results for multiple tools and samples in a single report. *Bioinformatics* **32**, 3047–3048 (2016).
23. Li, H. & Durbin, R. Fast and accurate short read alignment with Burrows-Wheeler transform. *Bioinformatics* **25**, 1754–1760 (2009).
24. García-Alcalde, F. et al. Qualimap: evaluating next-generation sequencing alignment data. *Bioinformatics* **28**, 2678–2679 (2012).
25. van der Auwera, G. A. et al. From FastQ data to high confidence variant calls: the Genome Analysis Toolkit best practices pipeline. *Curr. Protoc. Bioinformatics* **43**, 11.10.1–11.10.33 (2013).
26. Anders, S., Pyl, P. T. & Huber, W. HTSeq: a Python framework to work with high-throughput sequencing data. *Bioinformatics* **31**, 166–169 (2015).

27. Akbani, R. *MBatch*. https://github.com/MD-Anderson-Bioinformatics/MBatch (2018).
28. *GATK CalculateContamination*. https://gatk.broadinstitute.org/hc/en-us/articles/9570322332315-CalculateContamination (2023).
29. *MixChecker*. https://github.com/heinc1010/BAMixChecker (2022).
30. Lee, S. et al. NGSCheckMate: software for validating sample identity in next-generation sequencing studies within and across data types. *Nucleic Acids Res.* **45**, e103 (2017).
31. Adzhubei, I., Jordan, D. M. & Sunyaev, S. R. Predicting functional effect of human missense mutations using PolyPhen-2. *Curr. Protoc. Hum. Genet.* **7**, Unit7.20 (2013).
32. Wickham, H. et al. Welcome to the Tidyverse. *J. Open Source Softw.* **4**, 1686 (2019).
33. Baddeley, A. & Turner, R. spatstat: an R package for analyzing spatial point patterns. *J. Stat. Softw.* **12**, 1–42 (2005).
34. Zeileis, A. & Grothendieck, G. zoo: S3 infrastructure for regular and irregular time series. *J. Stat. Softw.* **14**, 1–27 (2005).
35. Ayers, M. et al. IFN-γ-related mRNA profile predicts clinical response to PD-1 blockade. *J. Clin. Investig.* **127**, 2930–2940 (2017).
36. Kaptein, P. et al. Addition of interleukin-2 overcomes resistance to neoadjuvant CTLA4 and PD1 blockade in ex vivo patient tumors. *Sci. Transl. Med.* **14**, eabj9779 (2022).
37. Spranger, S. et al. Tumor-residing Batf3 dendritic cells are required for effector T cell trafficking and adoptive T cell therapy. *Cancer Cell* **31**, 711–723.e4 (2017).
38. Danaher, P. et al. Gene expression markers of tumor infiltrating leukocytes. *J. Immunother. Cancer* **5**, 18 (2017).
39. Becht, E. et al. Estimating the population abundance of tissue-infiltrating immune and stromal cell populations using gene expression. *Genome Biol.* **17**, 218 (2016).
40. Liberzon, A. et al. The molecular signatures database (MSigDB) hallmark gene set collection. *Cell Syst.* **1**, 417–425 (2015).
41. Korotkevich, G. et al. Fast gene set enrichment analysis. Preprint at bioRxiv https://doi.org/10.1101/060012 (2021).
42. Hänzelmann, S., Castelo, R. & Guinney, J. GSVA: gene set variation analysis for microarray and RNA-seq data. *BMC Bioinformatics* **14**, 7 (2013).
43. Bolotin, D. A. et al. Antigen receptor repertoire profiling from RNA-seq data. *Nat. Biotechnol.* **35**, 908–911 (2017).
44. Rawson, R. V. et al. Pathological response and tumour bed histopathological features correlate with survival following neoadjuvant immunotherapy in stage III melanoma. *Ann. Oncol.* **32**, 766–777 (2021).
45. Morad, G. et al. Hallmarks of response, resistance, and toxicity to immune checkpoint blockade. *Cell* **184**, 5309–5337 (2021).
46. Nauseef, W. M., McCormick, S. J. & Clark, R. A. Calreticulin functions as a molecular chaperone in the biosynthesis of myeloperoxidase. *J. Biol. Chem.* **270**, 4741–4747 (1995).
47. Meissner, T. B., Li, A. & Kobayashi, K. S. NLRC5: a newly discovered MHC class I transactivator (CITA). *Microbes Infect.* **14**, 477–484 (2012).
48. Nelson, V., Davis, G. E. & Maxwell, S. A. A putative protein inhibitor of activated STAT (PIASy) interacts with p53 and inhibits p53-mediated transactivation but not apoptosis. *Apoptosis* **6**, 221–234 (2001).
49. Raghavan, M. et al. Calreticulin in the immune system: ins and outs. *Trends Immunol.* **34**, 13–21 (2013).
50. Kobayashi, K. S. & van den Elsen, P. J. NLRC5: a key regulator of MHC class I-dependent immune responses. *Nat. Rev. Immunol.* **12**, 813–820 (2012).
51. Rayanade, R. J. et al. Regulation of IL-6 signaling by p53: STAT3- and STAT5-masking in p53-Val135-containing human hepatoma Hep3B cell lines. *J. Immunol.* **161**, 325–334 (1998).
52. Hoefsmit, E. P. et al. Inhibitor of apoptosis proteins antagonist induces T-cell proliferation after cross-presentation by dendritic cells. *Cancer Immunol. Res.* **11**, 450–465 (2023).
53. Muir, C. A. et al. Thyroid immune-related adverse events following immune checkpoint inhibitor treatment. *J. Clin. Endocrinol. Metab.* **106**, e3704–e3713 (2021).
54. Newell, F. et al. Multiomic profiling of checkpoint inhibitor-treated melanoma: identifying predictors of response and resistance, and markers of biological discordance. *Cancer Cell* **40**, 88–102.e7 (2022).
55. Chen, P. L. et al. Analysis of immune signatures in longitudinal tumor samples yields insight into biomarkers of response and mechanisms of resistance to immune checkpoint blockade. *Cancer Discov.* **6**, 827–837 (2016).
56. Amaria, R. N. et al. Neoadjuvant immune checkpoint blockade in high-risk resectable melanoma. *Nat. Med.* **24**, 1649–1654 (2018).
57. Mittal, D. et al. New insights into cancer immunoediting and its three component phases - elimination, equilibrium and escape. *Curr. Opin. Immunol.* **27**, 16–25 (2014).
58. Gerlinger, M. et al. Intratumor heterogeneity and branched evolution revealed by multiregion sequencing. *N. Engl. J. Med.* **366**, 883–892 (2012).
59. Salmon, H. et al. Host tissue determinants of tumour immunity. *Nat. Rev. Cancer* **19**, 215–227 (2019).
60. Hegde, P. S. & Chen, D. S. Top 10 challenges in cancer immunotherapy. *Immunity* **52**, 17–35 (2020).
61. Papillon-Cavanagh, S. et al. Pan-cancer analysis of the effect of biopsy site on tumor mutational burden observations. *Commun. Med.***1**, 56 (2021).
62. Lucas, M. W. et al. The NADINA trial: a multicenter, randomised, phase 3 trial comparing the efficacy of neoadjuvant ipilimumab plus nivolumab with standard adjuvant nivolumab in macroscopic resectable stage III melanoma. *J. Clin. Oncol.* **40**, TPS9605 (2022).

Acknowledgements

We thank all the patients and their families for participation in the trials and the investigators and members of the clinical trial teams from NKI, MIA, and Karolinska Institute; the NKI-AVL Core Facility Molecular Pathology & Biobanking (CFMPB) for supplying NKI-AVL biobank material and laboratory support; and Alberto Gil-Jimenez for his help with the spatial analyses. A.M.M. is supported by an NHRMC Investigator Grant, Nicholas and Helen Moore, and Melanoma Institute Australia. N.M. is a recipient of a Postgraduate Research Fellowship 2022 from the Royal College of Pathologists of Australasia Foundation, a Research Training Program stipend scholarship from the University of Sydney, and a Melanoma Institute Australia Postgraduate Research scholarship. RAS is supported by a National Health and Medical Research Council of Australia (NHMRC) Investigator Grant (2022/GNT2018514). G.V.L. is supported by a National Health Medical Research Council Investigator Grant and the University of Sydney Medical Foundation.

Author contributions

J.M.V. and C.U.B. designed the study. JMV collected patient data, selected tumor samples, and analyzed and interpreted clinical and translational data, and wrote the first draft of the manuscript. N.M., R.A.S., and B.A.v.d.W. performed the revision of the pathologic response. H.S. and P.D. performed bioinformatics analyses. R.E. scored the immunofluorescence stainings, A.B. was responsible for the RNA isolations and performance of the staining of the biopsies. A.M.M., I.L.M.R., A.M.M.v.d.V., E.K., A.C.J.v.A., and G.V.L. treated patients within the trials and provided additional patient data for this study. T.N.S. provided valuable input on the project. All authors interpreted the data, reviewed the manuscript, and approved the final version.

Competing interests

The authors declare no direct conflicts with this work. For unrelated conflicts, AMM reported advisory board honoraria from Bristol-Myers Squibb, MSD, Novartis, Roche, Pierre-Fabre, and QBiotics. I.L.M.R. and P.D. reported financial interest in Signature Oncology, and will receive

some possible revenues if the IFNγ signature is being developed as a clinical companion diagnostic. A.M.M.v.d.V. reported consultancy honoraria (all paid to the institute) from Bristol-Myers Squibb, MSD, Eisai, Ipsen, Sanofi, Pierre Fabre, Pfizer, Novartis, and Roche. E.K. has consultancy/advisory relationships with Bristol Myers Squibb, Pierre Fabre, Immunocore and Lilly, and received research grants not related to this paper from Bristol Myers Squibb, Delcath, Novartis, and Pierre-Fabre. Not related to current work and paid to institute. RAS has received fees for professional services from IO Biotech ApS, MetaOptima Technology Inc., F. Hoffmann-La Roche Ltd, Evaxion, Provectus Biopharmaceuticals Australia, Qbiotics, Novartis, Merck Sharp & Dohme, NeraCare, AMGEN Inc., Bristol-Myers Squibb, Myriad Genetics, GlaxoSmithKline. BAvdW reported an advisory role for Bristol-Myers Squibb. A.C.J.v.A. has received advisory board and consultancy honoraria from Amgen, Bristol-Myers Squibb, MSD-Merck, Merck-Pfizer, Neracare, Novartis, Pierre Fabre, Provectus, Sanofi, Sirius Medical, and 4SC, all paid to the institute; and research grants received from Amgen, Bristol-Myers Squibb, Merck-Pfizer, and Novartis, all paid to the institute. TNS reported advisory roles for Allogene Therapeutics, Asher Bio, Merus, Neogene Therapeutics, Scenic Biotech, and Third Rock Ventures; and is a stockowner of Allogene Therapeutics, Asher Bio, Celsius, Merus, Neogene Therapeutics, Scenic Biotech, and Third Rock Ventures. G.V.L. reported consultant advisor roles for Agenus, Amgen, Array Biopharma, AstraZeneca, Bayer, BioNTech, Boehringer Ingelheim, Bristol-Myers Squibb, Evaxion, Hexal AG (Sandoz Company), Highlight Therapeutics, IOBiotech, Immunocore, Innovent Biologics USA, Merck Sharpe & Dohme, Novartis, PHMR Ltd, Pierre Fabre, Regeneron, Scancell, and SkylineDX. C.U.B. received compensation (all paid to the institute except TRV) for advisory roles for Bristol-Myers Squibb, MSD, Roche, Novartis, GSK, AZ, Pfizer, Lilly, GenMab, Pierre Fabre, Third Rock Ventures; received research funding (all paid to the institute) from Bristol-Myers Squibb, Novartis, NanoString, and declares stock ownership in Flindr Therapeutics (formerly Immagene BV), where he is co-founder. Financial support for the trials was provided by Bristol-Myers Squibb, with the Netherlands Cancer Institute as sponsor of the OpACIN, OpACIN-neo, and PRADO trials.

Additional information

Supplementary information The online version contains supplementary material available at https://doi.org/10.1038/s43856-025-01118-9.

Correspondence and requests for materials should be addressed to Christian U. Blank.

Peer review information *Communications Medicine* thanks Giuseppe Palmieri and the other anonymous reviewer(s) for their contribution to the peer review of this work.

Reprints and permissions information is available at http://www.nature.com/reprints

Publisher's note Springer Nature remains neutral with regard to jurisdictional claims in published maps and institutional affiliations.

[1]Department of Medical Oncology, Netherlands Cancer Institute, Amsterdam, the Netherlands. [2]Division of Molecular Oncology and Immunology, Netherlands Cancer Institute, Amsterdam, the Netherlands. [3]Core Facility Molecular Pathology and Biobanking, Netherlands Cancer Institute, Amsterdam, the Netherlands. [4]Melanoma Institute Australia, University of Sydney, Sydney, NSW, Australia. [5]Faculty of Medicine and Health, University of Sydney, Sydney, NSW, Australia. [6]Department of Medical Oncology, Royal North Shore and Mater Hospitals, Sydney, NSW, Australia. [7]Tissue Pathology and Diagnostic Oncology, Royal Prince Alfred Hospital and NSW Health Pathology, Sydney, NSW, Australia. [8]Departments of Medical Oncology and Radiology & Nuclear Medicine, Erasmus Medical Center, Rotterdam, the Netherlands. [9]Department of Medical Oncology, Leiden University Medical Center, Leiden, the Netherlands. [10]Charles Perkins Centre, University of Sydney, Sydney, NSW, Australia. [11]Department of Pathology, Netherlands Cancer Institute, Amsterdam, the Netherlands. [12]Department of Melanoma and Surgical Oncology, Royal Prince Alfred Hospital, Sydney, NSW, Australia. [13]Department of Hematology, Leiden University Medical Center, Leiden, the Netherlands.
✉e-mail: c.blank@nki.nl